Research Article | Vol. 25, No. 15 | 24 Jul 2017 | OPTICS EXPRESS 18378
Optics EXPRESS

Asymmetry of Raman scattering by structure variation in space

RIDONG WANG, PENGYU YUAN, MENG HAN, SHEN XU, TIANYU WANG, AND XINWEI WANG*

271 Applied Science Complex II, Department of Mechanical Engineering, Iowa State University, Ames, IA 50011, USA
**xwang3@iastate.edu*

Abstract: We report on the discovery of asymmetries of Raman scattering along one scanning direction, between two scanning directions, and by structure variation of the sample in space. Asymmetry of Raman shift along the *x* direction, and the asymmetry of Raman shift and linewidth between the two scanning directions (*x* and *y*) are found for a 1210 nm diameter silica particle. The observed asymmetries are confirmed by further 2D Raman scanning of the same particle. To further explore the asymmetry of Raman scattering, glass fibers of three diameters (0.53, 1.00, and 3.20 μm) are scanned along two directions. The asymmetry of Raman shift along each direction, the asymmetry of linewidth along the *y* direction, and the asymmetry of Raman shift and linewidth between the two scanning directions are discovered. Additionally, 11 nm-thick $MoSe_2$ nanosheets on silicon are used to discover whether an asymmetry of Raman scattering exists at the edge of the nanosheets. One edge of the nanosheet is scanned in four directions and the asymmetry of Raman scattering caused by the step variation is also detected. All the observed Raman scattering asymmetries are explained soundly by the Raman signal diffraction and image shift on the CCD detector arrays of the Raman spectrometer. In practice, to use scanning Raman for surface structure study, great measure has to be taken to consider the structure-induced asymmetries to uncover the real Raman wave number variation by intrinsic material structure. We propose a signal processing method by averaging the scanning points along four directions to eliminate the interference of the edge. This method works well to significantly suppress the asymmetries of Raman properties and uncover the real Raman signal change by structure variation.

OCIS codes: (300.6450) Spectroscopy, Raman; (290.5860) Scattering, Raman; (290.5850) Scattering, particles; (180.5810) Scanning microscopy; (160.4236) Nanomaterials.

References and links

1. D. A. Long, *Raman Spectroscopy* (Mcgraw-Hill, 1977).
2. P. Rostron, S. Gaber, and D. Gaber, "Raman Spectroscopy, Review," IJERT **6**(1), 50–64 (2016).
3. E. V. Efremov, F. Ariese, and C. Gooijer, "Achievements in resonance Raman spectroscopy review of a technique with a distinct analytical chemistry potential," Anal. Chim. Acta **606**(2), 119–134 (2008).
4. R. S. Das and Y. K. Agrawal, "Raman spectroscopy: recent advancements, techniques and applications," Vib. Spectrosc. **57**(2), 163–176 (2011).
5. S. A. Asher, "UV resonance Raman spectroscopy for analytical, physical, and biophysical chemistry. Part 2," Anal. Chem. **65**(4), 201A–210A (1993).
6. A. Kudelski, "Analytical applications of Raman spectroscopy," Talanta **76**(1), 1–8 (2008).
7. Y. Yue and X. Wang, "Nanoscale thermal probing," Nano Rev. **3**(1), 11586–11596 (2012).
8. A. Milani, M. Tommasini, V. Russo, A. Li Bassi, A. Lucotti, F. Cataldo, and C. S. Casari, "Raman spectroscopy as a tool to investigate the structure and electronic properties of carbon-atom wires," Beilstein J. Nanotechnol. **6**, 480–491 (2015).
9. L. M. Malard, M. A. Pimenta, G. Dresselhaus, and M. S. Dresselhaus, "Raman spectroscopy in graphene," Phys. Rep. **473**(5–6), 51–87 (2009).
10. M. D. Sonntag, E. A. Pozzi, N. Jiang, M. C. Hersam, and R. P. Van Duyne, "Recent advances in tip-enhanced Raman spectroscopy," J. Phys. Chem. Lett. **5**(18), 3125–3130 (2014).
11. C. C. Neacsu, S. Berweger, and M. B. Raschke, "Tip-enhanced Raman imaging and nanospectroscopy: sensitivity, symmetry, and selection rules," Nanobiotechnol. **3**(3-4), 172–196 (2007).
12. N. Kumar, S. Mignuzzi, W. Su, and D. Roy, "Tip-enhanced Raman spectroscopy: principles and applications,"

#297684 https://doi.org/10.1364/OE.25.018378
Journal © 2017 Received 12 Jun 2017; revised 15 Jul 2017; accepted 18 Jul 2017; published 20 Jul 2017

Optics EXPRESS

ERJ Tech. Instrum. **2**(1), 9 (2015).
13. B. Pettinger, P. Schambach, C. J. Villagómez, and N. Scott, "Tip-enhanced Raman spectroscopy: near-fields acting on a few molecules," Annu. Rev. Phys. Chem. **63**(1), 379–399 (2012).
14. S. Najjar, D. Talaga, L. Schue, Y. Coffinier, S. Szunerits, R. Boukherroub, L. Servant, V. Rodriguez, and S. Bonhommeau, "Tip-enhanced Raman spectroscopy of combed double-stranded DNA Bundles," J. Phys. Chem. **118**(2), 1174–1181 (2014).
15. X. Wang, D. Zhang, K. Braun, H. Egelhaaf, C. J. Brabec, and A. J. Meixner, "High-resolution spectroscopic mapping of the chemical contrast from nanometer domains in P3HT: PCBM organic blend films for solar-cell applications," Adv. Funct. Mater. **20**(3), 492–499 (2010).
16. E. M. V. S. Lantman, T. Deckert-Gaudig, A. J. G. Mank, V. Deckert, and B. M. Weckhuysen, "Catalytic processes monitored at the nanoscale with tip-enhanced Raman spectroscopy," Nat. Nanotechnol. **7**(9), 538–586 (2012).
17. N. Lee, R. D. Hartschuh, D. Mehtani, A. Kisliuk, J. F. Maguire, M. Green, M. D. Foster, and A. P. Sokolov, "High contrast scanning nano-Raman spectroscopy of silicon," J. Raman Spectrosc. **38**(6), 789–796 (2007).
18. Y. Okuno, Y. Saito, S. Kawata, and P. Verma, "Tip-enhanced Raman investigation of extremely localized semiconductor-to-metal transition of a carbon nanotube," Phys. Rev. Lett. **111**(21), 216101 (2013).
19. W. Su and D. Roy, "Visualizing graphene edges using tip-enhanced Raman spectroscopy," J. Vac. Sci. Technol. B **31**(4), 041808 (2013).
20. R. Zhang, Y. Zhang, Z. C. Dong, S. Jiang, C. Zhang, L. G. Chen, L. Zhang, Y. Liao, J. Aizpurua, Y. Luo, J. L. Yang, and J. G. Hou, "Chemical mapping of a single molecule by plasmon-enhanced Raman scattering," Nature **498**(7452), 82–86 (2013).
21. A. Lutz, I. De Graeve, and H. Terryn, "Non-destructive 3-dimensional mapping of microcapsules in polymeric coatings by confocal Raman spectroscopy," Prog. Org. Coat. **88**, 32–38 (2015).
22. J. M. Bobbitt, D. Mendivelso-Perez, and E. A. Smith, "Scanning angle Raman spectroscopy: A nondestructive method for simultaneously determining mixed polymer fractional composition and film thickness," Polymer (Guildf.) **107**, 82–88 (2016).
23. J. M. Englert, P. Vecera, K. C. Knirsch, R. A. Schäfer, F. Hauke, and A. Hirsch, "Scanning-Raman-Microscopy for the statistical analysis of covalently functionalized graphene," ACS Nano **7**(6), 5472–5482 (2013).
24. F. Liu, Y. Zhu, Y. Liu, X. Wang, P. Ping, X. Zhu, H. Hu, Z. Li, and L. He, "Real-time Raman microspectroscopy scanning of the single live sperm bound to human zona pellucida," Fertil. Steril. **99**(3), 684–689 (2013).
25. J. C. Hulteen and R. P. Van Duyne, "Nanosphere lithography: A materials general fabrication process for periodic particle array surfaces," J. Vac. Sci. Technol. A **13**(3), 1553–1558 (1995).
26. V. Ng, Y. V. Lee, B. T. Chen, and A. O. Adeyeye, "Nanostructure array fabrication with temperature-controlled self-assembly techniques," Nanotechnology **13**(5), 554–558 (2002).
27. J. Huang, A. R. Tao, S. Connor, R. He, and P. Yang, "A general method for assembling single colloidal particle lines," Nano Lett. **6**(3), 524–529 (2006).
28. C. Hsu, S. T. Connor, M. X. Tang, and Y. Cui, "Wafer-scale silicon nanopillars and nanocones by Langmuir-Blodgett assembly and etching," Appl. Phys. Lett. **93**(13), 133109 (2008).
29. S. Jeong, L. Hu, H. R. Lee, E. Garnett, J. W. Choi, and Y. Cui, "Fast and scalable printing of large area monolayer nanoparticles for nanotexturing applications," Nano Lett. **10**(8), 2989–2994 (2010).
30. Q. H. Wang, K. Kalantar-Zadeh, A. Kis, J. N. Coleman, and M. S. Strano, "Electronics and optoelectronics of two-dimensional transition metal dichalcogenides," Nat. Nanotechnol. **7**(11), 699–712 (2012).
31. K. Boussu, B. Van der Bruggen, A. Volodin, J. Snauwaert, C. Van Haesendonck, and C. Vandecasteele, "Roughness and hydrophobicity studies of nanofiltration membranes using different modes of AFM," J. Colloid Interface Sci. **286**(2), 632–638 (2005).

1. Introduction

Raman spectroscopy is a technique specialized in measuring the frequency shift of inelastic scattered light from the sample when the photon from the incident light strikes a molecule and produces a scattered photon [1–4]. The out coming scattered light can be a photon with a lower frequency than the original one and in that case, it is known as Stokes Raman scattering or with a higher frequency and known as anti-Stokes Raman scattering [5]. The shift in wavelength of the scattered light depends on the chemical composition of the molecules responsible for scattering. As a result, Raman spectrum can be treated as a fingerprint of different compounds [6]. It is also found that the temperature difference would lead to the difference in lattice vibration, thus, affects Raman signal in the form of intensity, frequency (Raman shift) and width of peaks (linewidth). This feature makes it possible for the Raman spectrum to be used in temperature measurement in a non-contact and non-destructive manner [7]. Additionally, Raman spectroscopy is also a useful tool for structure analysis. For

Optics EXPRESS

instance, this method could be used to detect the defects in carbon nanostructures, to identify the number of layers and the edge structure in graphene [8-9].

While Raman spectroscopy is very well suited for studying the composition and structure of materials, for temperature measurement, and for local structural variations, there are still some problems and interferences hidden in conventional microscopy studies due to the resolution limit imposed by diffraction [10]. Tip-enhanced Raman Spectroscopy (TERS) overcomes this limitation and provides nanoscale spatial resolution and improved detection sensitivity. TERS combines the high spatial resolution of scanning probe microscopy (SPM) with the chemical, structural, and temperature information obtained through Raman scattering [11-12]. The increase of the Raman signal is due to a strong field enhancement at the SPM tip apex related to the singular behavior of the electromagnetic field (akin to the lightning-rod effect) and localized surface plasmon resonance (LSPR) excitation for certain tip materials [13]. This technique has been used to study scientific problems in biology [14], photovoltaics [15], catalysis [16], semiconductors [17], carbon nanotubes [18], graphene [19] and single molecule detection [20].

Raman scattering is typically a very weak effect due to the non-resonant interaction of the exciting photons with the molecules involved in the scattering process. TERS combines Raman spectroscopy and SPM to enhance the Raman signal. A confocal Raman system could also be used to enhance the Raman signal by limiting the collection of fluorescence photons emitted from the focal plane, which is the natural enemy of Raman spectroscopy. Thus, the scanning confocal Raman system, which combines the confocal Raman spectrometer with an automated 3D sample stage, could also be used to study the composition and structure of the sample and measure the temperature variation of the sample. Lutz *et al.* designed a scanning confocal Raman system to obtain more detailed insight into the distribution of microcapsules into the polymeric coating matrix. The 2-dimensional mapping at different heights allows a 3-dimensional representation and can thus give more precise information about the location of the microcapsules within the coating [21]. Bobbitt *et al.* developed a scanning angle Raman spectroscopy to simultaneously measure the chemical composition and thickness of waveguide mixed polymer films with varying fractional compositions [22]. Englert *et al.* proposed a systematic method for the quantitative and reliable characterization of covalently functionalized graphene based on scanning Raman microscopy. This makes it possible to record and analyze several thousands of Raman spectra per sample and obtain various Raman properties and their correlations with each other in 2D-plots [23]. Liu *et al.* used real-time Raman microspectroscopy scanning technique to distinguish zona pellucida (ZP) bound sperm from unbound sperm. This technique could be further developed into a diagnostic tool to identify normal functional sperm [24].

A lot of research focused on the study of composition and structure of materials. The surface morphology of materials could also be detected based on Raman signal. However, the various asymmetries of Raman shift and linewidth caused by the morphology of materials, which are very important for accurate analysis, are not considered. In this research, a Raman scanning system which combines the confocal Raman system with a 3D scanning stage is set up to explore the morphology of nanomaterials, such as silica microparticles, glass micro fiber, and $MoSe_2$ nanosheet. Asymmetry of Raman scattering signal due to structure variation in space is discovered. The physics behind this asymmetry is interpreted in detail. This technique could be very promising for exploring the structure variation in space for different kinds of nanomaterials and for studying the phonon-structure interaction of different materials.

2. Raman asymmetry uncovered by near-field effect of silica microparticles

As shown in Fig. 1(a), the Raman scanning experiments are conducted using a confocal Raman system, which consists of a CW laser, a Raman spectrometer (Voyage^{TM}, B&W Tek, Inc.), a microscope (Olympus BX51), a 3D piezo-actuated nano-stage (ThorLabs MAX 312),

Optics EXPRESS

and a step-motor based neutral density filter (CONEX-NSR1). A longitudinal single mode laser of 532 nm is introduced to the system and its power is adjusted by the filter. A 100 × objective lens (NA = 0.80) is used in the microscope to obtain a small laser beam with a diameter of about 600 nm [Fig. 1(b)]. The 3D piezo-actuated nano-stage with a resolution of 20 nm is used to realize the focusing of the laser beam on the samples and 2-D scanning of the samples. The travel range of the stage is 20 μm in each direction. During the experiment, the Raman spectrometer, the filter and the 3D piezo-actuated nano-stage are all controlled by a LabVIEW-based software on the computer to shorten the experiment time, reduce the environmental interference to the system and improve the accuracy of the experiment.

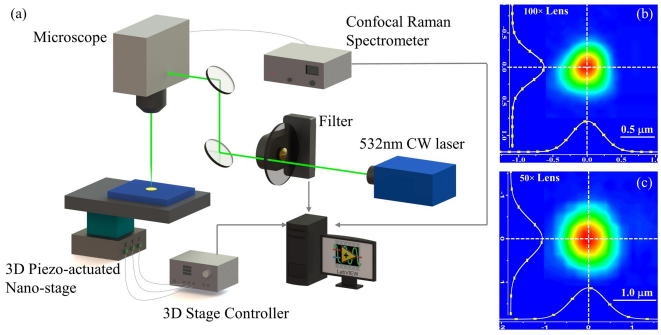

Fig. 1. Schematic of the confocal Raman scanning system with automatic Raman acquisition, energy tuning, and position scanning. (a) The sample is illuminated by a CW 532 nm (2.33 eV) green laser. The Raman signals are excited by the same laser and collected by a confocal Raman spectrometer (Voyage, B&W Tek, Inc.) with a spectral resolution of 1.05 ~1.99 cm^{-1}. The laser power is adjusted by a step-motor neutral density filter. The 3D nano-stage is used to realize scanning of the sample in different directions. The spectrometer, filter and the nano-stage are controlled by LabVIEW-based software. (b)(c) The spatial energy distribution of the laser beam. The diameter of the laser beam on the sample is determined as 1.2 μm under 50 × objective, and 0.6 μm under 100 × which are 1/*e* radius of the laser intensity profile.

2.1 Sample preparation

Samples are prepared by laying monolayer silica particles on silicon wafers, where the near-field heating is generated because of the particle-focused laser illumination. Many methods, such as spin-coating [25], tilting method [26], dip coating [27], Langmuir-Blodgett deposition [28], and wire-wound rod coating [29], could be used to realize deposition of silica microparticles on the silicon wafer. In this work, the spin-coating method is used to deposit silica microparticles on the silicon substrate. Surfactant (triton-X: methanol = 1:400 by volume) is mixed with monodisperse silica particle suspension. The surfactant is used to assist in wetting the surface of silicon substrate. The suspension has silica particles with a solid percentage of 10% suspended in water. Silica microparticles with a diameter of 1210 nm (Bangs Laboratories, Inc.) are used in the experiment without any surface treatment. The silicon substrates (University Wafer) are cleaned in acetone and then deionized water for one hour with ultrasonic agitation. To obtain a better arrangement of the microparticles, it is important to keep these silicon substrates in deionized water until they are used for microparticles deposition. The silicon substrate is then placed on the rotating stage of the spin coater (KW-4A, Chemat Technology Inc.). The mixture is dispersed onto the silicon substrate using a microliter syringe and the substrate is spun for 1 min with a speed of 1000 rpm. Then the silicon substrate with silica suspension is left to dry for about half an hour in the air. It is the hydrodynamic pressure that makes the silica microparticles layers form on the silicon substrate. Areas of monolayer particles can be found by using the scanning electron microscope (SEM). Figure 2(a) shows a SEM image of silica particles with a diameter of

Optics EXPRESS

1210 nm assembled on the silicon substrate via the spin-coating method. In the figure, there are some areas of single silica particles, which are used in the experiment.

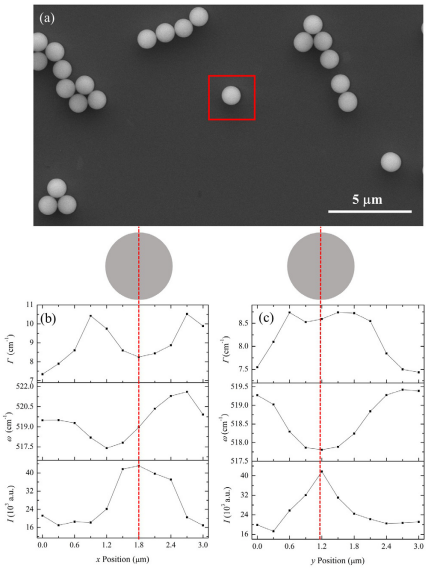

Fig. 2. (a) A scanning electron microscope image of silica microparticles with a diameter of 1210 nm deposited on the silicon wafer. (b) 1D Raman scanning results of 1210 nm single silica microparticle along the *x* direction. (c) 1D Raman scanning results of 1210 nm single silica microparticle along the *y* direction. The particle's location relative to the coordinate is shown in the figure.

2.2 Experimental results and discussion

In our experiment, the sample is placed on the 3D piezo-actuated nano-stage. The laser power is adjusted to 15 mW, and the Raman integration time is 0.1 s. The incident laser is focused by the objective lens on the silica microparticle. The laser beam is further focused on the silicon substrate by the microparticle. The excited Raman scattering signal is collected through the Raman spectrometer. In the experiment, it is very important to focus the laser beam on the silica particle to achieve high accuracy and precision of Raman signal. As a result, the stage is moved in the *z* direction with a step of 1 μm and the Raman signal is collected. Then a quadratic fitting method is used to obtain a good focal level of the laser based on Raman intensity~*z* relation. The sample is then scanned in a length of 3 μm with a step of 300 nm along the *x* and *y* directions, respectively. Note the *x* direction for scanning is the same for all samples, and the same for the *y* direction.

The Raman intensity I, Raman shift ω, and linewidth Γ of silicon vary along the two directions are shown in Figs. 2(b) and 2(c). Along the *x* direction, the intensity difference between I_{max} and I_{min} is 26.24×10^3, with a maximum intensity ratio (I_{max}/I_{min}) of 2.549. The maximum intensity appears when the laser beam is irradiating the center of the particle. ω changes in a range from 517.40 to 521.60 cm^{-1}, with a maximum shift of 4.20 cm^{-1}. Γ changes from 7.34 to 10.52 cm^{-1}, with a maximum difference of 3.18 cm^{-1}. Along the *y* direction, the intensity difference between I_{max} and I_{min} is 24.43×10^3, with a maximum intensity ratio (I_{max}/I_{min}) of 2.413. ω changes in a range from 517.80 to 519.42 cm^{-1}, with a maximum shift of 1.62 cm^{-1}. Γ changes from 7.43 to 8.73 cm^{-1}, with a maximum difference of 1.30 cm^{-1}. Two Raman property asymmetries are observed here. One asymmetry is with respect to the center position of the particle. Figures 2(b) and 2(c) shows that the variations of I and Γ along the two directions are symmetrical, the variation of ω along the *y* direction is symmetrical, while along the *x* direction is asymmetrical. We name this type of asymmetry

Optics EXPRESS

Type I asymmetry. The other asymmetry is between the scanning direction x and y. The particle is spherical and the induced near-field focusing should have the same distribution along the x and y directions. However, asymmetry exists for all the three Raman properties, and is most prominent for ω and Γ when comparing the variations of these three parameters between the two directions. We name this type of asymmetry Type II asymmetry. Along the two directions, the maximum intensity ratios are very close. The maximum shift of ω and the maximum difference of Γ along the x direction are around 2.5 times the values along the y direction.

To have a better understanding of the asymmetry uncovered above, 2D Raman scanning of a single silica microparticle is conducted in a range of 4.5 μm × 4.5 μm with a step of 300 nm. The scanning starting position is also adjusted three times in each direction with a step of 100 nm. Then, the best one is chosen to further verify whether the asymmetry exists in ω and Γ along different scanning directions. As shown in Fig. 3(a), the variations of Raman intensity along the two directions are very similar. The maximum intensity ratios of the two directions are both around 3.7, which indicates that the morphology of the silica microparticle could be reflected based on the result of Raman intensity. For ω, Fig. 3(b) clearly confirms the Type I asymmetry: it is asymmetrical along the x direction, but is symmetrical along the y direction. For Type II asymmetry (between x and y), it exists for both ω and Γ. The maximum shifts of ω along x and y directions are 4.8 cm^{-1} and 2.4 cm^{-1}, respectively, which means that the variations of ω along the two directions are asymmetrical. Though the maximum differences of Γ along x and y directions are nearly the same, both of which are around 3.0 cm^{-1}, and the variation of Γ along each direction is symmetrical, the asymmetry of Γ could be seen when comparing the variations between the two different directions (x and y).

As shown in Figs. 3(a)-3(c), the variations of the three parameters (I, ω and Γ) are very small when the laser beam is not irradiating the silica microparticle. It indicates that the effect of laser asymmetry could be ignored. Additionally, the beam path of incident laser is fixed. Thus, the observed asymmetry of Raman scattering can be explained by the microparticle induced near-field focusing effect as shown in Figs. 4(a) and 4(b). The schematic layout of optical systems together with the Raman spectrometer's CCD detector array is shown in Fig. 4(a). In Raman experiment, the Raman signal from the light focusing beam on the sample in fact is collected by the optical system and gives an image on the CCD detector. The intensity of all the detection pixels along the y direction at one x-location is added up to give the Raman intensity at one Raman shift location in the experiment. When the focusing beam is changed on the substrate, its image will shift on the CCD detector. Therefore, the measured Raman intensity, Raman shift, and linewidth will change accordingly. When the laser beam is not irradiating the silica microparticle, the laser beam irradiates the silicon substrate directly. When the laser beam is irradiating the silica microparticle, as shown in Fig. 4 (b), the laser beam will be focused by the microparticle. At position 1 or position 4, only the left part of the laser is focused by the particle. Thus, the energy density of this part is larger, and the Raman intensity of silicon will increase. When the microparticle is moving to position 2, the silica microparticle is at the center of the laser beam, the laser is totally focused by the microparticle, and the energy intensity of the laser increases to the maximum value. Accordingly, the Raman intensity of silicon at this position also is the largest. With further moving of the silica microparticle to position 3 or position 5, only the right part of the laser will be focused, and the Raman intensity will begin to decrease. When the microparticle is out of the range of the laser beam, the Raman intensity will be equal to the value before the microparticle entering the laser beam. As Raman intensity is only related to the energy density of the laser beam on the silicon substrate, the scanning direction will not affect the variation of the Raman intensity. Thus, not only the variation of intensity along each direction is symmetrical, the variations between the two directions are also symmetrical.

However, the variations of Raman shift and linewidth along the x direction and y direction are different. If the silica microparticle is moving along the x direction, the Raman signals of

Optics EXPRESS

different positions are shown in Fig. 4(a). At position 1, the left part of the Raman signal is refracted by the right part of the silica microparticle. This part of Raman signal will shift left and be collected by the detection units at left. Therefore, the Raman shift of silicon will decrease. Due to the shift part of the Raman signal, the linewidth will be larger. With moving of the silica particle from left to right, more Raman signal will be refracted by the right part of the silica microparticle, the Raman shift of silicon will also continue to decrease, and linewidth will increase. Then, the left part of the Raman signal will be refracted by the left part of the microparticle, the Raman shift of silicon will begin to increase, while linewidth will begin to decrease. When moving to position 2, the silica microparticle is at the center of the laser beam, the Raman signal refracted by the microparticle is symmetric, and the obtained Raman shift and linewidth will be equal to that before the silica microparticle entering the laser beam. This is true for the Raman shift as shown in Fig. 3(b), but the linewidth is a little larger than that when the laser beam directly irradiates silicon substrate. This reflects the fact that some signal spot enlarging effect by the microparticle. From position 2 to position 3, the Raman signal will be refracted by the left part of the microparticle and shift to right, the Raman shift of silicon will begin to increase, and the linewidth will also increase. If the microparticle continues to move to right, only part of the Raman signal will be refracted by the microparticle, and shifts to right. Thus, the obtained Raman shift and linewidth will decrease. When the microparticle is moved to a position where the Raman signal will not be refracted by the microparticle, Raman shift and linewidth will decrease to the value as that at position 2. As a result, the variation of Raman shift along the x direction is not symmetrical, while the variation of linewidth along this direction is symmetrical. That is Type I asymmetry exists for ω along the x direction.

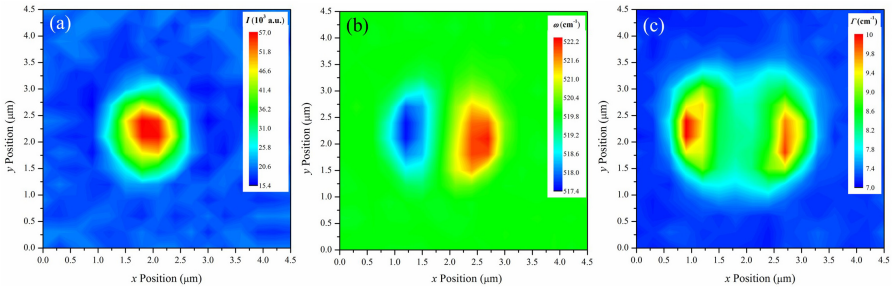

Fig. 3. (a) Raman intensity of 2D single silica microparticle scanning. (b) Raman shift of 2D single silica microparticle scanning. (c) Linewidth of 2D single silica microparticle scanning.

If the silica microparticle is moving along the y direction, the Raman signals will also be refracted by the silica microparticle following the same way described above. However, since the shift of the Raman signal is more along the y direction, the central position of the Raman peak will shift less than that in the x direction. The pixel numbers of detector along the x and y directions are 2048 and 122, respectively. This implies that with the moving of the sample along the y direction, the detector units in the y direction to collect the Raman signal are nearly the same. As a result, Raman shift and linewidth of silicon along this direction will change much less than the other direction. This can be proved by the Raman shift and linewidth variation along the y direction with x = 1.8 μm, which are shown in Figs. 3(b) and 3(c). The results shown in Fig. 2(c) show some variations of Raman shift since the scanning line may not be exactly passing the central point of the particle. When the scanning line is not exactly passing the center of the particle, the variations of ω and Γ are caused by the morphological variation along the x direction. Thus, the variations of ω and Γ are very small or symmetrical when the particle is scanned along the y direction, while the variations of ω and Γ between the two directions are asymmetrical. That is, there is no Type I asymmetry along this direction, while Type II asymmetry exists for both ω and Γ.

Optics EXPRESS

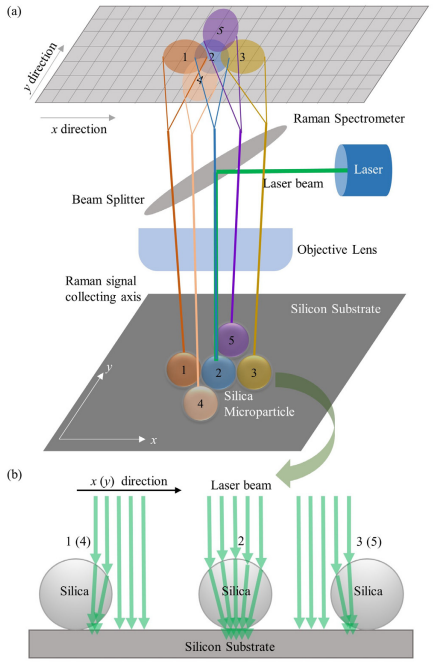

Fig. 4. Schematic of silica microparticle under laser illumination to explain the physics behind Raman asymmetry. (a) When the silica microparticle is moving along the x or y direction on the stage, different part of the particle is illuminated by the laser. The collected Raman signals of different positions are detected by different parts of the detector. (b) The laser focusing effect of silica microparticle at different positions.

3. Raman asymmetry by near-field effect of micro/sub-micron glass fibers

For silica microparticle, when the microparticle is scanned along one direction, the morphology variance along the other direction may also affect the Raman scanning results. To suppress this influence and further explore the asymmetry in ω and Γ along the two directions, single micro/sub-micron glass fibers with diameters of 0.53, 1.00 and 3.20 μm are also used with different layout orientations. These glass fibers provide more controlled scanning study since we can control their orientation relative to the scanning direction. The glass fibers of the three diameters are dispersed into alcohol with ultrasonic agitation. Then the solution is dropped onto the silicon substrate by a pipette. The sample is left in air to wait for alcohol to dry. At last, the glass fibers are attached to the surface of the silicon substrate. Figures 5(a)-5(c) show the SEM images of glass fibers attached to the silicon substrate. In our experiment, the glass fiber is oriented normal to the scanning direction.

The sample is placed on the 3D piezo-actuated nano-stage. The laser power is set to 13 mW, and the integration time is 0.1 s. The incident laser is focused by the objective lens on the glass fiber. Due to the optical effect of glass fiber, the laser beam is further focused on the silicon substrate. The 0.53 μm-thick glass fiber is scanned along the x direction in a range of 4 μm with a step of 100 nm. Then the sample is rotated by 90 degrees, and is scanned along the y direction. In this way, the same sample is scanned exactly in the same manner, but only along different directions. For the glass fiber with diameters of 1.00 and 3.20 μm, the scanning ranges are 4 and 9 μm, respectively. The scanning steps are 200 and 300 nm, respectively. As shown in Figs. 5(d)-5(i), the variations of Raman shift for different glass fibers along the two directions are also very small when the laser beam is irradiating the silicon substrate directly. That is, the effect of the laser asymmetry could also be ignored. The beam path of incident laser is the same as that used for the silica microparticles. Thus, the observed asymmetry of Raman scattering can be also explained by the micro/sub-micron

Optics EXPRESS

glass fiber induced near-field focusing. Figures 5(d)-5(i) show the variations of the Raman properties for all the three samples. The variations of Raman intensity along each direction of the three glass fibers are symmetric. The maximum intensity ratios (I_{max}/I_{min}) of the three glass fibers along the x direction are 1.70, 1.81, and 1.54, respectively, and I_{max}/I_{min} of the three glass fibers along the y direction are 1.64, 1.98, and 2.45, respectively. For glass fibers with diameters of 0.53 and 1.00 μm, the maximum intensity ratios between the two directions are very close. For the glass fiber with a diameter of 3.20 μm, the maximum intensity ratio along the y direction is larger than that along the x direction, which is due to the influence of the larger diameters on the focus of the laser beam. And the variation of linewidth along the x direction is also symmetric. The variations of Raman shift along the two scanning directions of the three glass fibers are asymmetrical with respect to the centerline of the fiber (Type I asymmetry). Type I asymmetry also exists for the variation of linewidth along the y direction.

However, for single silica microparticle, there is no Type I asymmetry for both ω and Γ variation along the y direction. This difference between the silica microparticles and glass fibers is caused by the surface morphology of the two materials. When the silica microparticle or glass fiber is scanned along the y direction, the change of detection units used to detect the Raman signal will change in both directions (x and y) in the Raman spectrometer due to the different variance of surface morphology. Because there are much more pixels along the x direction than that along the y direction, the small variation along the x direction will play a much more important role when the samples are scanned along the y direction. Comparing the variations of ω and Γ along the x direction with that along the y direction, Type II asymmetry also exists. The variations of ω and Γ along the x direction are much larger than that along the y direction. In addition, the diameters of the glass fibers could also be obtained based on the scanning results. As shown in Figs. 5(d)-5(i), the affected area diameters of the three glass fibers based on Raman intensity and Raman shift are around 1.25, 1.7, and 3.9 μm, respectively. After subtracting the diameter of laser beam, which is around 0.6 μm, the three values are very close to the diameters of the glass fibers obtained using SEM.

As shown in Figs. 5(d)-5(i), the change of Raman shift and linewidth will also increase with increased glass fiber diameter. When the glass fibers are scanned along the x direction, the maximum shifts of ω of the glass fibers with three different diameters are 0.99, 2.05, and 4.00 cm^{-1}, respectively. The maximum variations of Γ are 0.41, 0.95, and 4.40 cm^{-1}, respectively. When the glass fibers are scanned along the y direction, the maximum shifts of ω of the glass fibers with three different diameters are 0.20, 0.33, and 1.39 cm^{-1}, respectively. Raman signal refracted by the glass fiber with a larger diameter will go through a longer path in the glass fiber, and the shift of Raman signal after this glass fiber will also be larger. As a result, Raman shift and linewidth will change more when a thicker glass fiber is scanned. Figures 5(d) and 5(e) shows that when the laser beam is on the center of the glass fiber, the values of ω and Γ are close to the values when the glass fiber is not under the laser beam. However, as shown in Fig. 5(f), when the diameter of the glass fiber is 3.20 μm, the value of ω is close to that when the glass fiber is not under the laser beam, while the value of Γ is larger than that when the glass fiber is not under the laser beam. In the scanning experiment, the 3D stage is adjusted to focus the laser beam on the silicon substrate. When the glass fiber with a larger diameter is under the laser beam, the laser beam on the glass fiber will be out of focus, which will increase the linewidth, while ω will not change.

4. Type III asymmetry by nm-thick 2D material structure: $MoSe_2$

In the above Raman asymmetry study, the Raman signal is scattered by the structure at the micron or sub-micron scales. To further investigate this structure-induced asymmetry, we use ~10 nm thick multilayered $MoSe_2$ samples. The samples are obtained using the mechanical exfoliation method [30] from bulk $MoSe_2$ crystals. Adhesive Scotch tape and gel films (Gel-Film, PF-20/1.5-X4, Gel-Pak) are used to transfer the $MoSe_2$ nanosheet to a clean silicon substrate. The $MoSe_2$ nanosheet on silicon is identified by using the optical microscope,

Optics EXPRESS

atomic force microscope (AFM) (NMAFM-2, Digital Instruments, CA, USA) and Raman spectroscopy. Figure 6(a) shows the AFM image of the sample on a silicon substrate. As shown in Fig. 6(b), the sample has a thickness of about 11 nm. This image is obtained under the contact mode, which is beneficial to measure the thickness of the sample with a high resolution [31]. Then the sample is mounted on the 3D nano-stage and the edge is located using the optical microscope of the confocal Raman system. The edge of the nanosheet is scanned in the *x* and *y* directions (with the edge normal to the scanning direction). For each direction, the sample is scanned both from the silicon substrate to the $MoSe_2$ nanosheet and from the $MoSe_2$ nanosheet to the silicon substrate. Both the Raman signal of silicon substrate and $MoSe_2$ nanosheet are obtained.

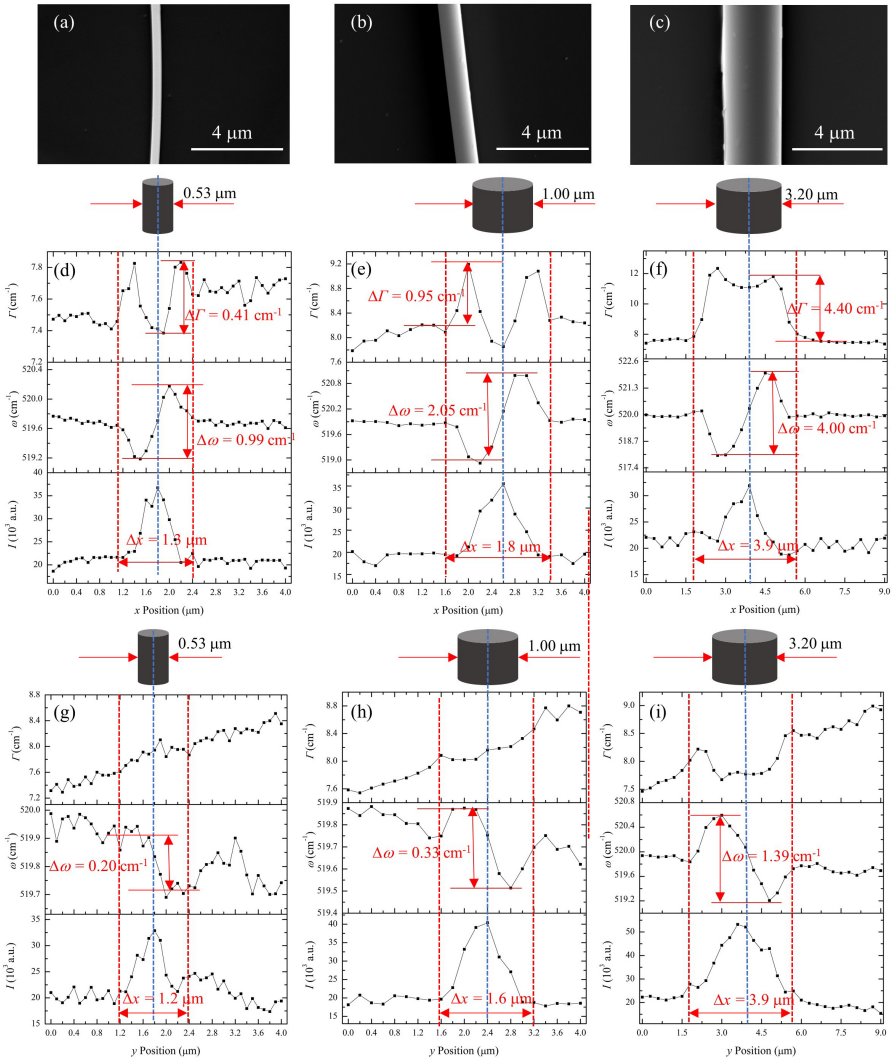

Fig. 5. (a)-(c) SEM images of single glass fibers on the silicon substrate (0.53 μm, 1.0 μm, and 3.20 μm). (d)-(i) 1D Raman scanning results of glass fiber with the three diameters along two (*x* and *y*) directions. The red dashed lines indicate the boundaries of the affected areas of the glass fibers based on Raman intensity and Raman shift, and the blue dashed lines indicate the center of the glass fibers.

Optics EXPRESS

In the experiments, the laser power is adjusted to about 6.6 mW to give sufficient Raman signal while inducing moderate sample heating. A 50 × objective lens (NA = 0.50) is used in the microscope to obtain a small laser beam with a diameter of about 1.2 μm [Fig. 1(c)]. The integration time for obtaining the Raman signal of silicon substrate and $MoSe_2$ nanosheet are 0.5 s and 3 s, respectively. Figures 6(c)-6(f) show the four results of silicon substrate's Raman signal scanned in the four situations. Along the four directions, all the Raman intensity differences between I_{max} and I_{min} are around 14.9×10^3, with maximum intensity ratios (I_{max}/I_{min}) of about 5.5. The maximum intensity appears when the whole laser beam is irradiating on the silicon substrate. With the moving of the sample, more and more parts of the laser beam will first irradiate the nanosheet, which will decrease the energy intensity on the silicon. The corresponding Raman intensity will continue to decrease until the whole laser spot is on the nanosheet. When the nanosheet is moved along the x direction, the variances of ω are 0.95 and 1.1 cm^{-1}. While the variances of ω are 0.3 and 0.2 cm^{-1} when the nanosheet is moved along the y direction. Obviously, Type II asymmetry exists for ω. Additionally, with the moving of the sample along the x or y direction, another type of asymmetry exists for ω when the relative position of the laser beam changes from the silicon substrate to the nanosheet, and from the nanosheet to the silicon substrate. We name this type of asymmetry Type III asymmetry. Though the variation of detection units used to collect Raman signal will also affect linewidth, the variances of linewidth along the four directions are all very small, which indicates that the temperature variance of silicon is very small during the scanning process.

Figure 7(a) shows the optical scattering variation to explain the Raman properties' change observed in Fig. 6(c). At position 1, a small part of the laser beam is on the right side of nanosheet. Thus, only a small part of the Raman signal on the left part will be weakened by the $MoSe_2$, which makes the position of Raman peak shift to right. As a result, Raman shift will increase. At position 2, half of the laser beam is on the nanosheet, which leads to half of the Raman signal be weakened by the nanosheet. The maximum value of Raman shift will be obtained at this position. When more than half part of the laser beam is on the nanosheet, only a small part of the Raman signal on the right will not be weakened. The position of Raman peak on the CCD sensor will begin shifting to left, and the corresponding Raman shift of silicon will decrease until the whole laser beam is on the nanosheet (position 3), where the value of Raman shift will be equal to that before the nanosheet entering the laser beam. As shown in Fig. 6(d), more and more parts of the laser beam will irradiate the silicon directly when the laser beam position is moving from the nanosheet to the substrate along the x direction. As a result, the corresponding Raman intensity will continue to increase until the whole laser beam is on the silicon substrate. For the variation of Raman shift, when the whole laser beam is on the nanosheet, Raman signal will be decreased by the nanosheet before collected by the spectrometer. But due to the symmetry of Raman signal at this point, the value of Raman shift will be equal to the value obtained when the whole laser beam is on the silicon substrate.

When part of the laser beam is moving out of the nanosheet, part of the Raman signal on the left will not be weakened by the nanosheet. The position of Raman peak will shift to the left on the CCD sensor, and the value of Raman shift will begin to decrease until half of the particle is out of the nanosheet. With much more parts of the laser beam out of the nanosheet, only a small part of the signal on the right will be weakened. Raman shift will begin to increase until the whole laser beam is on the silicon substrate. When the nanosheet is moved along the y direction, as the Raman intensity is only related to the energy density on the silicon, the variation of Raman intensity along the y direction is the same with that along the x direction. The variation of Raman shift along this direction is much smaller than that along the x direction, which is due to the detector. As shown in Fig. 6(c)-6(f), the maximum shift of ω along the x direction is around 1 cm^{-1} while the maximum shift of ω along the y direction is only about 0.25 cm^{-1}.

Optics EXPRESS

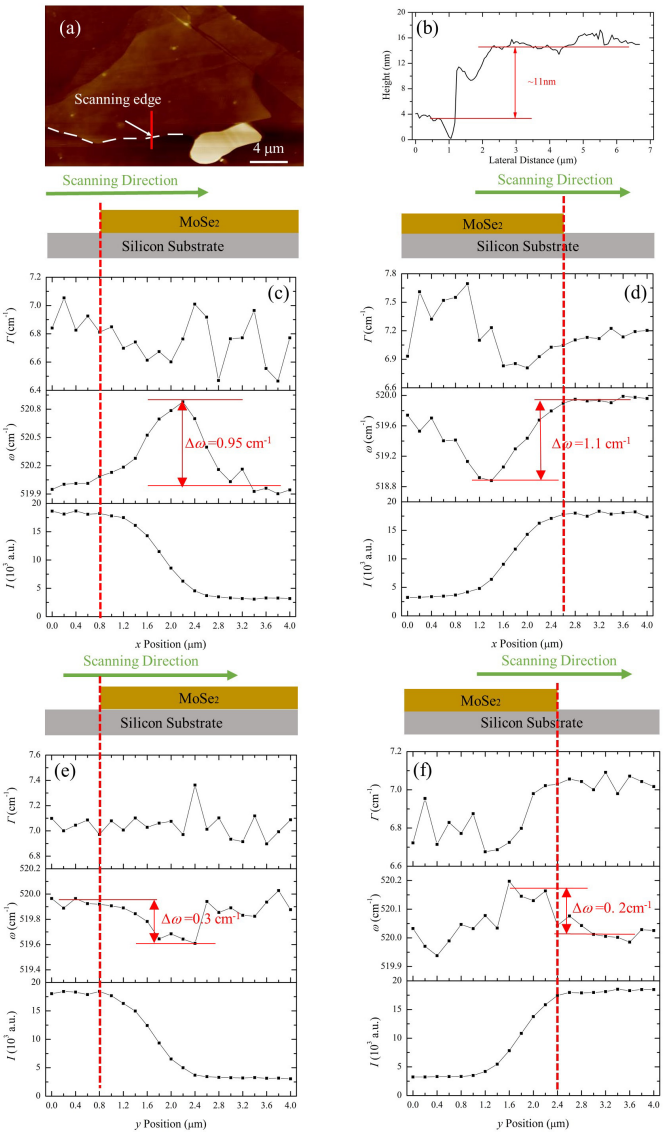

Fig. 6. AFM measurement results of $MoSe_2$ and 1D scanning results of the silicon Raman signal along four directions. (a) The 2D surface image of the sample. (b) The thickness of the sample obtained along the stage that is used for Raman scanning. (c) Scanning from silicon substrate to $MoSe_2$ nanosheet along the x direction. (d) Scanning from $MoSe_2$ nanosheet to silicon substrate along the x direction. (e) Scanning from silicon substrate to $MoSe_2$ nanosheet along the y direction. (f) Scanning from $MoSe_2$ nanosheet to silicon substrate along the y direction.

Figures 8(a)-8(d) show the four results of $MoSe_2$ nanosheet scanned in four directions. As Raman intensity is only related to the energy density of the laser, when the laser beam is moving from silicon substrate to the nanosheet, the Raman intensity will increase until the whole laser beam is on the nanosheet and will decrease until the whole laser beam is moving out of the nanosheet. As shown in Figs. 8(a)-8(d), the variances of ω along the x direction are 1.75 and 1.55 cm^{-1} while the variances of ω along the y direction are 0.9 and 0.3 cm^{-1}. This indicates that Type II asymmetry exists for ω. In addition, Type III asymmetry also exists for ω. As when the sample is moved along the x or y direction, the variations of ω are not

Optics EXPRESS

symmetrical when the relative position of the laser beam changes from the silicon substrate to the nanosheet, and from the nanosheet to the silicon substrate. The variations of linewidth along the four directions are also very small, which indicates that the temperature variance of $MoSe_2$ nanosheet is very small during the scanning process.

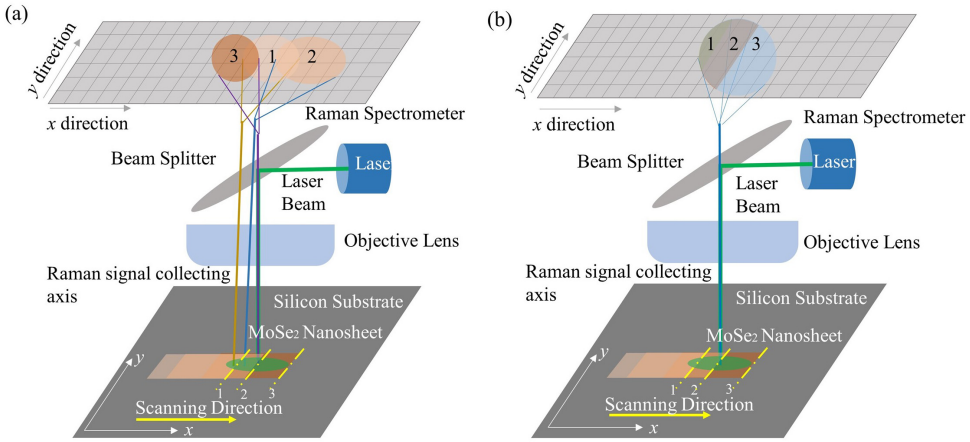

Fig. 7. (a) Schematic of the scanning Raman system used to detect the Raman signal of silicon substrate. (b)Schematic of the scanning Raman system used to detect the Raman signal of $MoSe_2$ nanosheet.

Figure 7(b) shows the optical scattering variation to explain the Raman properties' change observed in Fig. 8(a). At position 1, a small part of the laser beam is on the right side of nanosheet. Only a small part of the Raman signal of $MoSe_2$ on the far left will be collected by the Raman spectrometer. At position 2, half of the laser beam is on the nanosheet, which will make the left half of the Raman signal be collected and the position of Raman peak will shift to right. Consequently, the obtained ω will increase. With moving of the sample, part of the Raman signal on the right will also be collected, and ω will continue to increase. The maximum value of Raman shift will be obtained when the nanosheet is moved to position 3, where the whole laser beam is irradiating on the nanosheet. When the $MoSe_2$ nanosheet is rotated 180°, and is still moved along the x direction, the relative position of the laser beam will be moving from the nanosheet to the silicon substrate. With moving of the nanosheet, the left end of the laser beam will be out of the nanosheet, and irradiate on the silicon substrate. As a result, the Raman signal will begin to shift right, and the obtained ω will increase until the whole part of the laser beam is irradiating the silicon substrate, when there is no Raman signal of the nanosheet. When the nanosheet is moved along the y direction, the variation of Raman shift along this direction is much smaller than that along x direction. With moving of the sample stage, the shape of the laser beam on the nanosheet is changing, which will also change the energy distribution of the laser spot on the nanosheet. As a result, the variation of Raman shift along the four directions will not only be affected by the variance of detection units used to collect the Raman signal, but also the continuous changing of the shape of the laser beam. When the nanosheet is moved along the x direction, the variation of detection units plays a major role in the variance of the Raman shift, while the variation of the laser beam will play a leading role when the nanosheet is moved along the y direction. As shown in Figs. 8(a)-8(d), the maximum shifts of ω along x direction are both around 1.6 cm^{-1} while the maximum shifts of ω along y direction are 0.9 and 0.3 cm^{-1}, respectively.

Optics EXPRESS

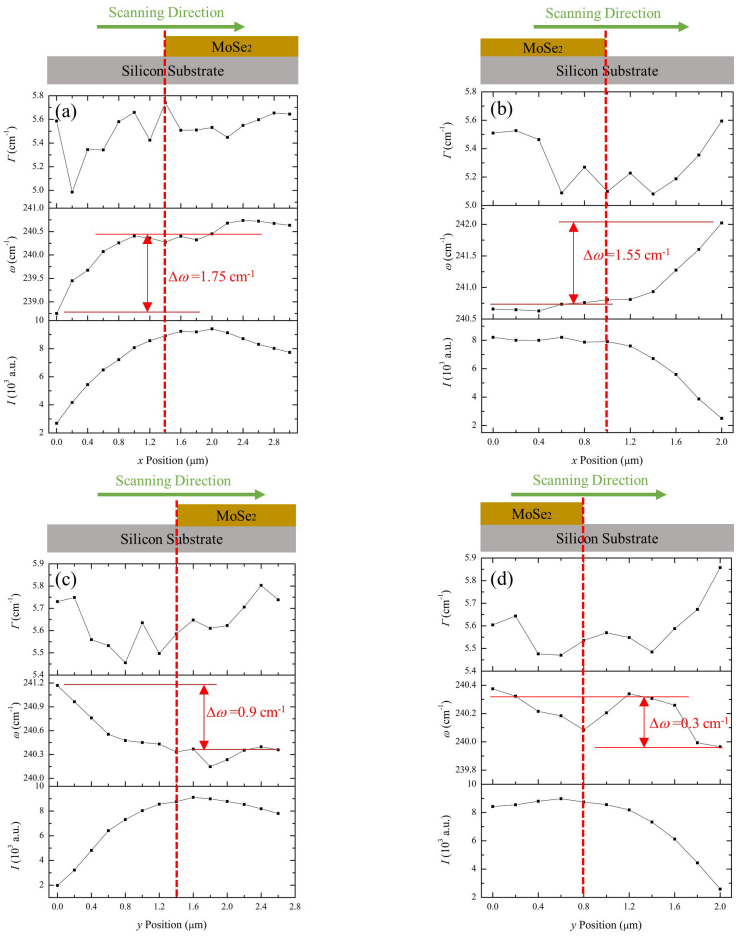

Fig. 8. 1D scanning results of $MoSe_2$ Raman signal along four directions. (a) From silicon substrate to $MoSe_2$ nanosheet along the x direction. (b) From $MoSe_2$ nanosheet to silicon substrate along the x direction. (c) From silicon substrate to $MoSe_2$ nanosheet along the y direction. (d) From $MoSe_2$ nanosheet to silicon substrate along the y direction.

As shown in Figs. 6(c)-6(f), and Figs. 8(a)-8(d), the variations of I and ω are very small when the laser beam is totally irradiating the silicon substrate, or the $MoSe_2$ nanosheet, which also indicates that the effect of the laser asymmetry could be ignored. The beam path is also the same with that used for silica microparticles and micro/sub-micron glass fibers. Thus, only the effect of asymmetries among different scanning directions should be considered to obtain a much more accurate Raman scanning results. The average of the scanning results along $-x$ and $+x$ directions, or along $-y$ and $+y$ directions could eliminate the Type III asymmetry. And the average of the scanning results along $-x$ and $-y$ directions, or along $+x$ and $+y$ directions could eliminate the Type II asymmetry. As a result, both Type II and Type III asymmetries could be eliminated when the Raman signals along the four directions at the corresponding positions are averaged. As shown in Figs. 9(a) and 9(b), the variation of Raman intensity and linewidth are still the same after averaging, which indicate that Raman intensity is only related to energy density of the laser beam and the temperature variance is very small during the scanning process. The maximum shift of ω after data reconstruction is only about 0.20 cm^{-1}, which is much smaller than that before data reconstruction. Thus, the asymmetry of Raman scattering along different directions has a big effect on the results of

Optics EXPRESS

Raman shift and should be eliminated before exploring the sample using Raman scanning method.

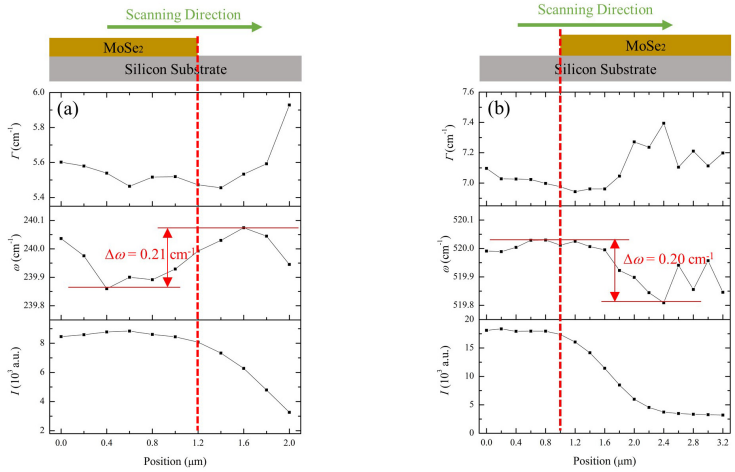

Fig. 9. Raman scanning results of $MoSe_2$ nanosheet and silicon substrate after signal reconstruction. (a) Results of $MoSe_2$ Raman signal with the relative position of laser beam moving from nanosheet to substrate. (b) Results of silicon Raman signal with the relative position of laser beam moving from substrate to nanosheet.

5. Conclusion

In summary, asymmetries of Raman scattering along one scanning direction, between two scanning directions, and by structure variation of sample in space were discovered. Silica microparticles with a diameter of 1210 nm, glass fibers of different diameters, and $MoSe_2$ were deposited on the silicon substrate to explore the effect of the asymmetry on the experimental results. It was found that the variance of Raman intensity was symmetric. For silica microparticle, both the variance of Raman shift along the *x* direction, and the variances of Raman shift between the two scanning directions were asymmetric. The variance of linewidth along each scanning direction was symmetric while asymmetry was found when comparing the scanning results along the two scanning directions. For glass fibers, the asymmetry of Raman shift not only existed along each scanning direction, but also could be discovered when comparing the scanning results of the two directions. And asymmetries of linewidth were observed when the glass fibers were scanned along the *y* direction, and comparing the scanning results along the two directions. The asymmetries mentioned above were mainly caused by the alignment of the detector units in the spectrometer and the pixel numbers along each direction. For $MoSe_2$ nanosheet, in addition to the asymmetry of Raman shift when scanned along the two directions, a third asymmetry, which was caused by the step variation of the $MoSe_2$ nanosheet on silicon substrate, could also be found when the sample was scanned from the silicon substrate to $MoSe_2$ nanosheet and from $MoSe_2$ nanosheet to the silicon substrate along the same direction. A data construction method was proposed to eliminate these two kinds of asymmetries. In practice, if scanning Raman is used to explore the interaction effect between different materials, the asymmetries of Raman scattering caused by the boundaries of different materials should be considered seriously.

Funding

National Science Foundation (CBET1235852, CMMI1264399); Department of Energy (DENE0000671, DE-EE0007686); Iowa Energy Center (MG-16-025, OG-17-005).